Journal of Quantitative Spectroscopy & Radiative Transfer 133 (2014) 351–363

Contents lists available at ScienceDirect

Journal of Quantitative Spectroscopy & Radiative Transfer

journal homepage: www.elsevier.com/locate/jqsrt

Inverse transient radiation analysis in one-dimensional participating slab using improved Ant Colony Optimization algorithms

B. Zhang, H. Qi *, Y.T. Ren, S.C. Sun, L.M. Ruan

School of Energy Science and Engineering, Harbin Institute of Technology, 92, West Dazhi Street, Harbin 150001, PR China

ARTICLE INFO

Article history:
Received 19 April 2013
Received in revised form
27 August 2013
Accepted 29 August 2013
Available online 5 September 2013

Keywords:
Inverse problem
Ant Colony Optimization
Transient radiative transfer
Finite Volume Method

ABSTRACT

As a heuristic intelligent optimization algorithm, the Ant Colony Optimization (ACO) algorithm was applied to the inverse problem of a one-dimensional (1-D) transient radiative transfer in present study. To illustrate the performance of this algorithm, the optical thickness and scattering albedo of the 1-D participating slab medium were retrieved simultaneously. The radiative reflectance simulated by Monte-Carlo Method (MCM) and Finite Volume Method (FVM) were used as measured and estimated value for the inverse analysis, respectively. To improve the accuracy and efficiency of the Basic Ant Colony Optimization (BACO) algorithm, three improved ACO algorithms, *i.e.*, the Region Ant Colony Optimization algorithm (RACO), Stochastic Ant Colony Optimization algorithm (SACO) and Homogeneous Ant Colony Optimization algorithm (HACO), were developed. By the HACO algorithm presented, the radiative parameters could be estimated accurately, even with noisy data. In conclusion, the HACO algorithm is demonstrated to be effective and robust, which had the potential to be implemented in various fields of inverse radiation problems.

1. Introduction

Inverse radiation analysis is concerned with the determination of the radiative properties, the temperature profile or source term distribution from various types of radiation measurements. It is very practical and useful in many different fields, e.g., optical tomography in medical imaging, laser-based nondestructive testing, remote sensing of the atmosphere and the prediction of the temperature distribution of highly luminous flame [1]. Recently, a number of papers have examined various inverse radiation problems on determining the scattering albedo, optical thickness, absorption coefficient, scattering coefficient, boundary condition or scattering phase function from various types of radiation measurements [2–10].

Meanwhile, a wide variety of solution techniques have been successfully employed in these inverse radiation analyses, which can be roughly grouped into two categories. One is the traditional algorithm based on gradient such as the conjugate gradient (CG) method [11,12], and Levenberg–Marquardt (L–M) method [13,14], etc. The other is the intelligent optimization algorithm such as genetic algorithm (GA) [15,16] and particle swarm optimization (PSO) algorithm [7,17], etc. However, all these traditional methods depend on the initial value, iteration step and the differentiability of the objective function, and the gradients which are difficult to be solved accurately by numerical simulation in some cases [1]. Furthermore, for the multidimensional nonlinear combinatorial optimization problems with constrained conditions, the traditional algorithms based on gradient are hard to get the global

* Corresponding author. Tel.: +86 451 86412638.
E-mail address: qihong@hit.edu.cn (H. Qi).

0022-4073/$ - see front matter © 2013 Elsevier Ltd. All rights reserved.
http://dx.doi.org/10.1016/j.jqsrt.2013.08.020

Nomenclature

c the speed of light
d_i the length of the path of the ith inversed parameter
$down_i(t)$ the minimum value of the hunting zone of the ith inversed parameter at iteration t
$feature_{i,\ j}(t)$ the characteristic value of the jth subinterval of the ith inversed parameter at iteration t
H Heaviside function
$high_i$ the high limit of initial search space of the ith inversed parameter
$iter$ the number of iterations
I_0 the peak radiation intensity of the incident laser, $W/(m^2\ sr)$
$I_c(t)$ the radiation intensity of incident laser at time t, $W/(m^2\ sr)$
I^- the radiation intensity when $0 \le \theta < \pi/2$, $W/(m^2\ sr)$
I^+ the radiation intensity when $\pi/2 < \theta \le \pi$, $W/(m^2\ sr)$
L the length of the media, m
low_i the low limit of the initial search space of the ith inversed parameter
N the total number of inversed parameters
N_c the maximum number of the iterations
N_l the total number of the measurement positions
N_m the total number of the common ants
N_n the total number of the divisions of the hunting zone
N_r the total number of the stochastic ants
N_s the total number of samples in each time step using MCM
N_x the total number of the grids
N_θ the total number of the polar angles
O^k objective function
$P^k_{i,\ j}(t)$ the probability of ant k selecting the jth path of the ith searching at iteration t
Q the pheromone concentration
$R(t^*)$ the reflectance on the left boundary at dimensionless time t^*
$\Delta range_i(t)$ the size of the subinterval of the ith inversed parameter at iteration t
$rand_n$ standard normal distributed random number
$rand_u$ uniform random number in [0, 1]
t time or iteration in ACO algorithm
$tabu^k_i(t)$ tabu list of ant k of the ith searching at iteration t
t_p laser pulse width, s
Δt^*_{fvm} the dimensionless time step in FVM
Δt^*_{mcm} the dimensionless time step in MCM
$up_i(t)$ the maximum value of the hunting zone of the ith inversed parameter at iteration t
$\mathbf{X}^k(t)$ the path array of the kth ant at iteration t
$x^k_i(t)$ the path selected by the kth ant in the ith searching at iteration t
$\mathbf{X}_{best}$ the best-so-far path array
$x_{i,\ best}$ the best-so-far path of the ith searching
$\mathbf{X}_{1st}(t)$ the path array with the maximum value of heuristic information at iteration t
$x_{i,\ 1st}(t)$ the path with the first largest value of $[\tau_{i,j}(t)]^\alpha[\eta_{i,j}(t)]^\beta$ of the ith searching at iteration t
$x_{i,\ 2nd}(t)$ the path with the second largest value of $[\tau_{i,j}(t)]^\alpha[\eta_{i,j}(t)]^\beta$ of the ith searching at iteration t
$x_{i,\ 3rd}(t)$ the path with the third largest value of $[\tau_{i,j}(t)]^\alpha[\eta_{i,j}(t)]^\beta$ of the ith searching at iteration t
Y the retrieval variable
$\overline{Y}$ the mean value of retrieval variable
$\mathbf{Z}^k(t)$ the estimated value array
$z^k_l(t)$ the estimated value of the lth measurement position
$\mathbf{Z}^*$ the measured value array

Greeks symbols

α the factor of pheromone value
β the factor of heuristic information
χ the noise to signal ratio
ε the tolerance for minimizing the objective function
$\varepsilon_{m,\ abs}$ the maximum absolute error, %
$\varepsilon_{m,\ rel}$ the maximum relative error, %
ε_{rel} the relative error, %
Φ the scattering phase function
γ the measured errors, %
$\eta_{i,\ j}(t)$ the heuristic information of the jth path of the ith searching at iteration t
$\Delta\eta^k_{i,\ j}(t)$ the heuristic information increased by ant k on the jth path of the ith searching at iteration t
κ_e extinction coefficient, m^{-1}
κ_s scattering coefficient, m^{-1}
θ polar angle
ρ evaporation rate
σ standard deviation
τ optical thickness or pheromone value
$\tau_{i,\ j}(t)$ the pheromone value on the jth path of the ith searching at iteration t
$\Delta\tau^k_{i,\ j}(t)$ the increased pheromone value deposited by ant k on the jth path of the ith searching at iteration t
ω single scattering albedo
$\mathbf{\Omega}$ radiation direction
Ω solid angle, sr
ξ the limit of the smallest size of subintervals
ζ the homogeneous factor

Subscripts

exa the exact value of the measured value or retrieved variable
i the searching index
j the subintervals index
k the ants index
l the measurement position index
L the value at $x=L$
L_2 norm-L_2

s	the pheromone value or heuristic information of the probability formula on the sth path
Superscripts	
k	the ants index
m	the scattering direction or outgoing direction
m'	the incoming direction
T	matrix transpose
$*$	the dimensionless term

optimal solution [18]. Compared to the traditional gradient based methods, the intelligent optimization algorithms do not rely on the analytic character of the objective function, and have good optimization abilities in harsh conditions such as the objective function is discontinuous and non-differentiable [19]. It encourages scholars to apply the intelligent optimization algorithms successfully to inverse radiation problems, even though they are prone to fall into local convergence, lack of strict mathematical theory, and heavily dependent on experience.

Similar to the above intelligent optimization algorithms, the Ant Colony Optimization (ACO) algorithm is a potential heuristic bionic evolutionary algorithm. It was first proposed in 1991 by the Italian scholar Dorigo [20] from the observation of the foraging behavior of real ants. Since 1996, ACO algorithm had drawn the attention of scholars from many countries all over the world, and its application fields were rapidly expanded. In 2000, Gutjahr [21] proved the convergence of ACO algorithm for the first time. In the same year, Dorigo and Bonabeau [22] gave a review of ACO algorithm in *Nature*, and pushed the ACO algorithm to the international academic front. In 2004, Dorigo and Stützle [23] published a book, *Ant Colony Optimization*, which is regarded as the authoritative resource on the ACO algorithm. At present, the ACO algorithm has a large number of applications in the following areas: traveling salesman problem [24,25], scheduling problem [26,27], continuous function optimization [28,29], data mining [30,31], target assignment [32–34], etc.

However, to the authors' best knowledge, there were few reports concerning on the application of ACO algorithm to the inverse transient radiation analysis. In the development of the ACO algorithm, a lot of research shows that ACO algorithm has the following advantages [23]: (1) positive feedback: in the process of foraging, the shorter the foraging path is, the more pheromone ants deposit, at the same time, the more pheromone there is, the higher probability ants select; (2) parallelism: ant colony is a distributed system, which means the ant's searching process is independent from each other, and ants only communicate via the pheromones instead of directly contacting with each other; (3) robustness: a single ant's wrong behavior can barely affect the whole system, not only is it easy to be combined with other algorithms, but it can be applied to other practical problems by making simple alterations.

In this paper, we attempted to apply the ACO algorithms to the inverse transient radiation problem. A one-dimensional (1-D) homogeneous semi-transparent gray slab medium was investigated. The optical thickness and scattering albedo were retrieved simultaneously by measuring the reflectance on the boundary. The influences of optimal results with measured errors were studied. Three improved ACO algorithms, including Region Ant Colony Optimization (RACO), Stochastic Ant Colony Optimization (SACO) and Homogeneous Ant Colony Optimization (HACO), were developed on the basis of the Basic Ant Colony Optimization (BACO). Compared with other algorithms, the HACO algorithm was demonstrated to be more effective and robust. The remainder of this paper is organized as follows: the original ACO algorithm and its variants are described in Section 2. The detailed computational procedures of BACO algorithm are presented in Section 3. Several algorithms are used to estimate the optical thickness and scattering albedo of the transient radiative transfer in Section 4. The main conclusions and perspectives are provided in Section 5.

2. Theoretical model of ACO algorithm

As social insects, the behaviors of individual ants are simple and random, but they can carry out complex activities, and manifest certain intelligence. Biologists found that ants could always find the shortest path from the nest to the food sources during the foraging through the long-time observation. The reason is that ants deposit pheromone, an evaporable material, on the path they passed. From the view of probability, ants tend to select the path with higher pheromone value. The ACO algorithm was inspired by the intelligent behavior of real ant colonies [35].

2.1. Original ACO algorithm

The first ACO algorithm was introduced to solve the discrete domain optimization problem [36]. It was abstracted from the phenomenon that ants go back to the nest to move reinforcements after finding food, as illustrated in Fig. 1, in which the path through all food sources is a solution of optimization problem. Compared with the real ants, not only can artificial ants deposit pheromone according to the distance and amount of food, but they can also record their past behavior and know the total number of the food sources.

The basic elements of ACO technique are briefly stated and defined as follows:

Path $\mathbf{X}^k(t)$: It is an N-dimensional vector, which is a candidate solution to the inverse problem, where N is the number of the optimization variables in the inverse problem. For our inverse transient radiative model, path $\mathbf{X}^k(t)$ denotes the candidate optical thickness and

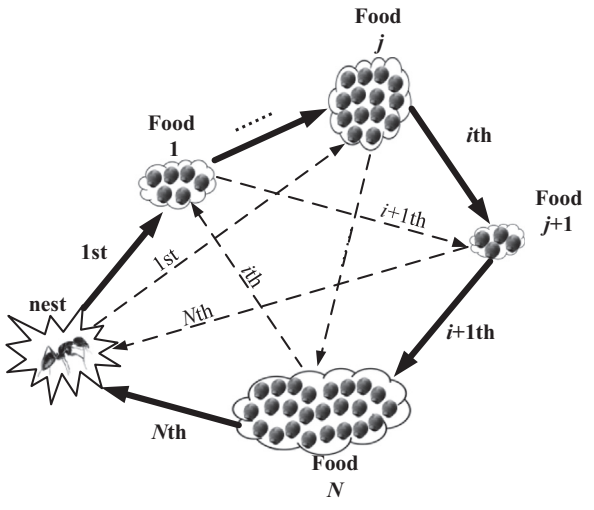

Fig. 1. The schematic diagram of the ants foraging.

scattering albedo. At iteration t, the path $\mathbf{X}^k(t)$ of ant k can be described as $\mathbf{X}^k(t)=[x_1^k(t), x_2^k(t), \ldots, x_N^k(t)]^{\mathrm{T}}$, where $x_i^k(t)$ is the solution component that ant k selected in the ith searching. For discrete domain optimization problem, the solution component refers to the food source, whereas for continuous domain optimization problem, it denotes the characteristic value of the subinterval.

Pheromone value $\tau_{i,j}(t)$: It is the pheromone value which depends on the quality of the solution component. At iteration t, $\tau_{i,j}(t)$ is the pheromone value of the jth food source during the ith searching or the pheromone value of the jth subinterval of the ith inverse parameter.

Heuristic information $\eta_{i,j}(t)$: It is the value of heuristic function which depends on the path selected by the ants. At iteration t, $\eta_{i,j}(t)$ is the heuristic information of the jth food source during the ith searching or the heuristic information of the jth subinterval of the ith inverse parameter.

Tabu list $tabu_i^k(t)$: It is the collection of food sources that the ant has found. At iteration t, $tabu_i^k(t)$ is the tabu list of ant k during the ith searching.

Probability formula $P_{i,j}^k(t)$: It is the probability of a path selected by ants. At iteration t, $P_{i,j}^k(t)$ is the probability that ant k selected the jth food source during the ith searching for discrete domain optimization problem, whereas it is the probability that ant k selected the jth subinterval of the ith inverse parameter for continuous domain optimization.

The original ACO algorithm can be summarized as follows:

(1) Input system data and control parameters, such as the size of the colony N_m, the factor of the pheromone value α, the factor of heuristic information β, the maximum number of the iterations N_c, the evaporation rate ρ and the pheromone concentration Q. Initialize the metabolic parameters during iterations, such as the pheromone value $\tau_{i,j}^k(t)$, the heuristic information $\eta_{i,j}^k(t)$ and the iteration $iter(t)$. Then clear the tabu list $tabu_i^k(t)$, and calculate the probability formula $P_{i,j}^k(t)$ to select the path $\mathbf{X}^k(t)$. The probability formula can be expressed as

$$P_{i,j}^k(t)=\begin{cases}\dfrac{[\tau_{i,j}(t)]^{\alpha}[\eta_{i,j}(t)]^{\beta}}{\sum_{s\notin tabu_i^k(t)}[\tau_{i,s}(t)]^{\alpha}[\eta_{i,s}(t)]^{\beta}}, & j\notin tabu_i^k(t)\\ 0, & j\in tabu_i^k(t)\end{cases} \tag{1}$$

where α and β are positive parameters which determine the relative importance of the pheromone value and the heuristic information. Modify the tabu list $tabu_{i+1}^k(t)$, if ant k selected the jth food source during the ith searching, the tabu list can be modified as shown below:

$$tabu_{i+1}^k(t)=tabu_i^k(t)\cup\{j\} \tag{2}$$

when ant k goes back to the nest, record the increased pheromone value $\Delta\tau_{i,j}^k(t)$ and heuristic information $\Delta\eta_{i,j}^k(t)$ on the path $\mathbf{X}^k(t)$ which ant k selected, they can be defined as follows:

$$\Delta\tau_{i,j}^k(t)=Q \tag{3}$$

$$\Delta\eta_{i,j}^k(t)=\frac{1}{d_i^k} \tag{4}$$

where Q is named as pheromone concentration which depends on the quality of food source. For example, if the quality of the food source is good, the pheromone concentration will be high. d_i^k is the length of the path selected by ant k during the ith searching. When all the ants finished searching, update the pheromone value and heuristic information as

$$\tau_{i,j}(t+1)=(1-\rho)\tau_{i,j}(t)+\sum_{k=1}^{N_m}\Delta\tau_{i,j}^k(t) \tag{5}$$

$$\eta_{i,j}(t+1)=\sum_{k=1}^{N_m}\Delta\eta_{i,j}^k(t) \tag{6}$$

where $\rho\in(0,1]$, which prevents the pheromone from gathering excessively when it is big enough. More ants slow down the convergence, whereas fewer ants reduce the accuracy. If the value of the objective function is less than those of all the previous paths, record the best-so-far path, which is also called the current optimal solution. We use the notation $\mathbf{X}_{best}=[x_{1,best}, x_{2,best}, \ldots, x_{N,best}]^{\mathrm{T}}$, where $x_{i,best}$ is the best-so-far path of the ith searching. Then complete one iteration.

(2) Repeatedly select the path according to the probability formula described by Eq. (1). Update the new pheromone value and heuristic information, using Eqs. (5) and (6), until the iteration number reaches a user-defined limit N_c, or the non-improvement of the best solution is obtained.

2.2. The Basic ACO algorithm for continuous optimization

Inverse transient radiation analysis is a continuous domain optimization problem. For the original ACO

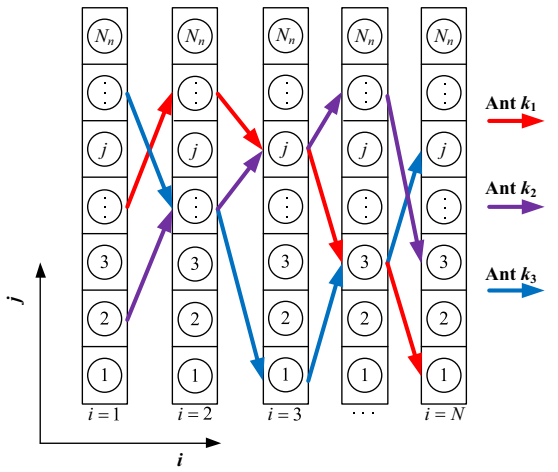

Fig. 2. The schematic diagram of selecting path by ant k in continuous domain.

algorithm is introduced to solve discrete problems, it cannot be applied directly and requires a local modification to adapt to this problem [37]. In contrast to the discrete optimization, the initial search space [low_i, $high_i$] of each inversed parameter needs to be estimated before optimizing, where low_i and $high_i$ denote the lower and upper limit of the initial search space, respectively. Each hunting zone is divided into N_n equal subintervals, where the center value of the subinterval is taken as the characteristic value, which means the value we used to represent the subinterval. Ant k selects path $\mathbf{X}^k(t)$ by probability formula as shown in Fig. 2.

The Basic ACO algorithm can be summarized as follows:

Input system data, such as the size of the colony N_m, the total portions of the hunting zone N_n, the factor of the pheromone value α, the factor of heuristic information β, the evaporation rate ρ and the pheromone concentration Q. Set the control parameters, such as the maximum number of the iterations N_c, the number of the inverse parameters N, the searching space of each inverse parameter [low_i, $high_i$], the tolerance for minimizing the objective function ε and the smallest size of the subinterval ξ. Initialize the metabolic parameters during iterations, such as the limits of the hunting zone $up_i(t)$ and $down_i(t)$, the pheromone value $\tau^k_{i,j}(t)$, the heuristic information $\eta^k_{i,j}(t)$ and the iteration $iter(t)$. Set the initial hunting zone [$down_i(t)$, $up_i(t)$] equal to the initial search space [low_i, $high_i$], and divide each hunting zone of N inversed parameters into N_n equal subintervals. Then calculate the probability formula $P^k_{i,j}(t)$ to select the path $\mathbf{X}^k(t)$ from the first inversed parameter to the Nth parameter. The probability formula is expressed as

$$P^k_{i,j}(t)=\frac{[\tau_{i,j}(t)]^\alpha[\eta_{i,j}(t)]^\beta}{\sum_{s=1}^{N_n}[\tau_{i,s}(t)]^\alpha[\eta_{i,s}(t)]^\beta} \tag{7}$$

When ant k goes back to the nest, calculate the objective function $O^k(t)$. Generally speaking, it can be defined as $O^k(t)=1/N_l||\mathbf{Z}^k(t)-\mathbf{Z}^*||_{L_2}$, where N_l is the total number of the measurement positions, $\mathbf{Z}^k(t)=[z^k_1(t), z^k_2(t), \ldots, z^k_{N_l}(t)]^{\mathrm{T}}$ is the estimated value calculated by the direct problem model, $\mathbf{Z}^*$ is the measured value. If the value of the objective function $O^k(t)$ is less than ever before, the best-so-far path will be recorded. Record the increased pheromone value $\Delta\tau^k_{i,j}(t)$ and heuristic information $\Delta\eta^k_{i,j}(t)$ on the path $\mathbf{X}^k(t)$ by which ant k selects, where $\Delta\tau^k_{i,j}(t)$ can be defined as Eq. (3), and $\Delta\eta^k_{i,j}(t)$ can be defined as follows:

$$\Delta\eta^k_{i,j}(t)=\frac{1}{N\,O^k(t)} \tag{8}$$

When all the ants complete searching, update the pheromone value and heuristic information as Eqs. (5) and (6), respectively. Reduce the hunting zone [$down_i(t+1)$, $up_i(t+1)$]. Take the subinterval, which makes the expression $[\tau_{i,j}(t)]^\alpha[\eta_{i,j}(t)]^\beta$ have the maximum value, of each inversed parameter as the best path at this iteration $\mathbf{X}_{1\mathrm{st}}(t)=[x_{1,1\mathrm{st}}(t), x_{2,1\mathrm{st}}(t), \ldots, x_{N,1\mathrm{st}}(t)]^{\mathrm{T}}$, then the hunting zone can be reduced as below:

$$down_i(t+1)=\begin{cases} x_{i,1\mathrm{st}}-\frac{up_i(t)-down_i(t)}{4}, & x_{i,1\mathrm{st}}-\frac{up_i(t)-down_i(t)}{4}>low_i \\ low_i, & otherwise \end{cases} \tag{9}$$

$$up_i(t+1)=\begin{cases} x_{i,1\mathrm{st}}+\frac{up_i(t)-down_i(t)}{4} & x_{i,1\mathrm{st}}+\frac{up_i(t)-down_i(t)}{4}<high_i \\ high_i & otherwise \end{cases} \tag{10}$$

Divide the new hunting zone of each inversed parameter into N_n equal subintervals. Based on the center values of the new subintervals and the old ones, calculate $\tau_{i,j}(t+1)$ and $\eta_{i,j}(t+1)$ in the next iteration by piecewise interpolation. Then complete one iteration. Repeatedly select the path according to the probability formula described by Eq. (7), reduce the hunting zone by using Eqs. (9) and (10), and update the new pheromone value and heuristic information, using Eqs. (5) and (6), until the program matches one of the following three stop criterions:

(a) The objective function reaches the setting accuracy ε, $O^k(t)<\varepsilon$.
(b) The size of the subinterval of hunting zone of each inversed parameter reaches a small specified positive number ξ, $\Delta range_i<\xi$, $(i=1, 2, \ldots, N)$.
(c) The number of the iteration reaches the user-defined iteration limit N_c, $iter(t)>N_c$.

where $\Delta range_i(t)$ denotes the size of subinterval of the hunting zone of the ith inversed parameter at iteration t, $\Delta range_i(t)=(up_i(t)-down_i(t))/N_n$, $iter(t)$ denotes the number of the iteration.

2.3. The improved ACO algorithms

Although the ACO algorithm has three outstanding advantages mentioned above, the BACO algorithm has its own defects. First of all, in the BACO algorithm, the ants select the path according to the pheromone value, and the pheromone value on the path which ants select will increase accordingly. This kind of algorithm has been termed 'greedy' in [35]. Thus, the optimization process is

easy to sink into local convergence, and fail to find the true global optimal value. Secondly, the reducing rule of the hunting zone is too mechanical, and the true global optimal value is easy to jump out of the hunting zone. Finally, due to the coupling effect between the inversed parameters, the BACO algorithm often leads to stagnation in the middle or latter periods of the optimization process.

2.3.1. The Region Ant Colony Optimization algorithm

The reducing rule of hunting zone in BACO algorithm is very mechanical, which reduces to half of its size after each iteration centered on the maximum value of $[\tau_{i,j}(t)]^{\alpha}[\eta_{i,j}(t)]^{\beta}$. Due to the coupling effect between the inversed parameters, one or several true value of them may jump out of the hunting zone in the optimization process of multiple parameters, which can lead to the miss of the true value of the inversed parameter. Thus, we developed a RACO algorithm, whose reducing rule of hunting zone is determined by the paths with the first three largest values of $[\tau_{i,j}(t)]^{\alpha}[\eta_{i,j}(t)]^{\beta}$ and the best-so-far path $\mathbf{X}_{best}$, which can reduce the probability of true value jumping out of the hunting zone. In addition, when the number of the subintervals with the largest values is large, the convergence speed is slow, and when the number is small, the inversion accuracy is low.

In contrast to the BACO algorithm, the reducing rule of the RACO algorithm can be expressed as

$$down_i(t+1) = \min\{x_{i,1st}(t),\ x_{i,2nd}(t),\ x_{i,3rd}(t),\ x_{i,best}\} - \frac{\Delta range_i(t)}{2} \tag{11}$$

$$up_i(t+1) = \max\{x_{i,1st}(t),\ x_{i,2nd}(t),\ x_{i,3rd}(t),\ x_{i,best}\} + \frac{\Delta range_i(t)}{2} \tag{12}$$

where $x_{i,1st}(t)$, $x_{i,2nd}(t)$ and $x_{i,3rd}(t)$ denote the path of the ith inversed parameter with the first, second and third largest value of $[\tau_{i,j}(t)]^{\alpha}[\eta_{i,j}(t)]^{\beta}$, respectively.

2.3.2. The Stochastic Ant Colony Optimization algorithm

In the models described above, the path is fixed in one subinterval, the center of which is always taken as the characteristic value, which will lead to reducing the probability of selecting the true value. Therefore, a SACO algorithm was developed by adding a few ants which take a random location in the subinterval as the characteristic value. For the stochastic ants can search more locations in the subinterval, it alleviates the stagnation of the optimal results effectively. Due to increasing the amount of the ants, the searching time will increase at each iteration accordingly. The amount of the stochastic ants N_r is unsuitable if it is too big, and the amount is recommended to be set as $N_r = N_m/N_n + 1$.

Unlike the RACO algorithm, stochastic ants in the SACO algorithm take the characteristic value of the subinterval as

$$feature_{i,j}(t) = down_i(t) + (j - rand_u)\Delta range_i(t) \tag{13}$$

where $feature_{i,j}(t)$ is the characteristic value of the jth subinterval of the ith inversed parameter at iteration t, and $rand_u$ is an uniform random number in [0, 1].

2.3.3. The Homogeneous Ant Colony Optimization algorithm

One of the main reasons to lead the ACO algorithm to local convergence is the excessive use of the greed rules, which results in the gathering of pheromone almost in a single subinterval, and leaving very little pheromone to other subintervals. This is bad for the global optimization. Hence, based on the SACO algorithm, a HACO algorithm was developed by adding a homogeneous factor ζ.

In contract to the SACO algorithm, the homogeneous factor makes the probability of each subinterval greater than zero, and the probability formula in the HACO algorithm can be defined as follows:

$$P^k_{i,j}(t) = \frac{\zeta}{N_n} + (1-\zeta)\frac{[\tau_{i,j}(t)]^{\alpha}[\eta_{i,j}(t)]^{\beta}}{\sum_{s=1}^{N_n}[\tau_{i,s}(t)]^{\alpha}[\eta_{i,s}(t)]^{\beta}} \tag{14}$$

where ζ is a parameter in [0, 1].

3. Computation procedures of the BACO algorithm

The implementation of the approach for solving the inverse transient radiation problem by using the BACO algorithm can be carried out according to the following routine.

Step 1. Input system data, such as N_m, N_n, α, β, ρ and Q; input the control parameters of the inverse transient radiation problem, such as N_c, N, low_i, $high_i$, ε and ξ; initialize the alterable parameters during iterations, such as $up_i(t)$, $down_i(t)$, $\tau^k_{i,j}(t)$, $\eta^k_{i,j}(t)$, $iter(t)$.

Step 2. Calculate probability formula $P^k_{i,j}(t)$ using Eq. (7). After ant k selects the path according to $P^k_{i,j}(t)$, calculate $\mathbf{Z}$ by the direct problem model, and obtain the objective function $O_k(t)$, then recode $\Delta\tau^k_{i,j}(t)$ and $\Delta\eta^k_{i,j}(t)$ using Eqs. (3) and (8). If the value of the objective function is less than the previous one, save the best-so-far path $\mathbf{X}_{best}$. Furthermore, check the stop criterion (a), if the value is less than the given parameter ε, go to step 5, otherwise, go to the next step.

Step 3. After all the ants have selected the paths, update the hunting zone $[down_i(t), up_i(t)]$ using Eqs. (11) and (12). Check the stop criterion (b), if the size of the subinterval of hunting zone of each inversed parameter is less than the given parameter ξ, go to step 5, otherwise, update $\tau_{i,j}(t+1)$ and $\eta_{i,j}(t+1)$ using Eqs. (5) and (6).

Step 4. Divide the new hunting zone of each inversed parameter into N_n equal subintervals. Based on the center values of the new subinterval and the old, calculate $\tau_{i,j}(t+1)$ and $\eta_{i,j}(t+1)$ in the next iteration by piecewise interpolation. Check the stop criterion (c), if the number of the iterations reaches the given parameter N_c, go to step 5, otherwise, set $iter(t+1) = iter(t)+1$, and loop to step 2.

Step 5. Print out the optimal solution $\mathbf{X}_{best}$ to the inverse transient radiation problem, stop the program.

The computational procedure of the BACO algorithm is shown in Fig. 3. For the main differences of the RACO, SACO and HACO algorithms have been introduced in Section 2.3, here we will not repeat them.

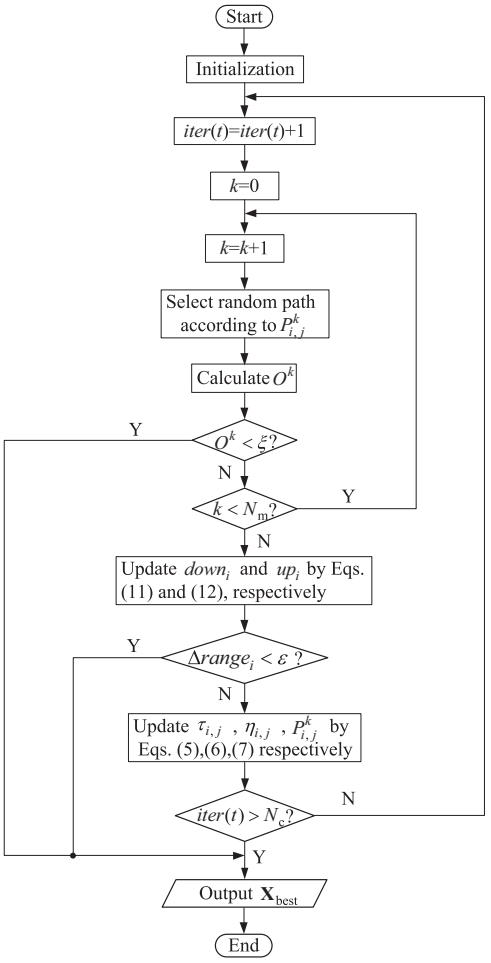

Fig. 3. The flowchart of the BACO algorithm.

4. Inverse transient radiation analysis by the ACO algorithms

To demonstrate the validity of the ACO algorithms in inverse transient radiation analysis, a test case of a 1-D homogeneous semi-transparent gray slab medium model was used in the present study. The optical thickness and scattering albedo were retrieved simultaneously to illustrate the performance of these algorithms. The case was implemented using FORTRAN code and the developed program was executed on an Intel Core i7-2600 PC. The accuracies and efficiencies of these algorithms were compared with each other in order to analyze the characteristics of each algorithm.

4.1. The description of the case

Let us consider the transient radiative transfer in a homogeneous absorbing and isotropic scattering but non-emitting plane-parallel slab with thickness L as shown in Fig. 4. The left surface of the slab ($x=0$) is exposed to a normally collimated and monochromatic incident Gaussian pulse. The index of refraction of the slab is assumed to be identical to that of the surroundings and equal to unity.

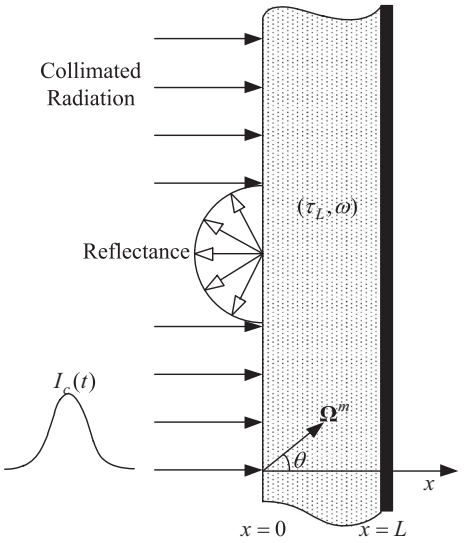

Fig. 4. The schematic of radiative transfer in a slab exposed to a normally collimated incident Gaussian pulse laser.

Thus the entire incident light is transmitted through the left surface and internal reflection can be ignored. The right surface of the slab ($x=L$) is supposed to be black and cold.

The incident radiation intensity on the left surface (at $x=0$) is a truncated Gaussian distribution with a pulse width t_p expressed as

$$I_c(t) = I_0 \exp\left[-4\ln 2\left(\frac{t}{t_p}-3\right)^2\right][H(t)-H(t-6t_p)] \tag{15}$$

where I_0 is the peak radiation intensity of the incident laser. $H(t)$ is Heaviside function, when $t>0$, $H(t)=1$; when $t<0$, $H(t)=0$.

4.2. Direct problem

Define the dimensionless time $t^*=\kappa_e ct$, where κ_e is the extinction coefficient, and c is the speed of light in the media. When substituting with the dimensionless parameters optical thickness τ and scattering albedo ω, the 1-D transient radiative transfer equation can be written as

$$\frac{\partial I(\tau,\mathbf{\Omega}^m,t^*)}{\partial t^*}+\mu\frac{\partial I(\tau,\mathbf{\Omega}^m,t^*)}{\partial \tau} = -I(\tau,\mathbf{\Omega}^m,t^*)+\frac{\omega}{4\pi}\int_{\Omega^{m'}=4\pi} I(\tau,\mathbf{\Omega}^m,t^*)\Phi(\mathbf{\Omega}^{m'},\mathbf{\Omega}^m)\,d\Omega^{m'} \tag{16}$$

where I is the intensity of the radiation, which is a function of position τ, direction $\mathbf{\Omega}^m$, and time t^*. τ is defined as $\tau=\kappa_e x$. μ is the direction cosine. ω is defined as $\omega=\kappa_s/\kappa_e$. $\Phi(\mathbf{\Omega}^{m'},\mathbf{\Omega}^m)$ is the scattering phase function between incoming direction $\mathbf{\Omega}^{m'}$ and scattering direction $\mathbf{\Omega}^m$. Ω is the solid angle, sr.

The boundary condition of the slab depicted in Section 4.1 can be expressed as

$$I^+(0,\theta,t^*)=\begin{cases} I_c(t^*), & \theta=0 \\ 0, & 0<\theta<\pi/2 \end{cases} \tag{17}$$

$$I^-(\tau_L,\theta,t^*)=0,\quad \pi/2<\theta\le\pi \tag{18}$$

where $I^+(0,\theta,t^*)$ denotes the intensity to the internal medium from the left side of the wall, and $I^-(\tau_L,\theta,t^*)$ denotes the intensity to the internal medium from the right side of the wall. θ is the polar angle, which is defined as the angle between the $\mathbf{\Omega}^m$ and positive x axis.

When the simultaneous radiative transfer equation and boundary conditions are solved, the radiative intensity on the border $I^-(0,\theta,t^*)$ can be obtained by numerical method, such as Finite Volume Method (FVM) and Monte-Carlo Method (MCM).

To validate the direct problem model, the medium physical parameters are set the same as which in the reference [38]. The optical thickness of the slab τ_L is 0.5, the scattering albedo ω is 0.7, and the dimensionless width of incident laser pulse t_p^*, which is defined as $t_p^*=\kappa_e c t_p$, is 0.15. The time-resolved transient hemispherical reflectance $R(t^*)$ is calculated within the dimensionless time $t^*<4$, where $t^*=\kappa_e ct$. It can be computed based on the following definition:

$$R(t^*)=2\pi\int_{\pi/2}^{\pi}\frac{I^-(0,\theta,t^*)}{I_0}\cos\,\theta\,\sin\,\theta\,d\theta \tag{19}$$

where $I^-(0,\theta,t^*)$ denotes the intensity to the external environment from the left side of the wall at time t^*.

The FVM and MCM were used to solve the time-resolved transient hemispherical reflectance. The result is shown in Fig. 5. In the FVM approximation, the number of grids was set as $N_x=5000$, the number of the polar angle was set as $N_\theta=100$, and the dimensionless time step was set as $\Delta t_{fvm}^*=0.0001$. In the MCM, the dimensionless time step was set as $\Delta t_{mcm}^*=0.04$, and the number of samples in each time step was set as $N_s=10^8$.

As can be seen from Fig. 5, the results calculated based on the FVM and MCM are in good agreement with reference [38], and the accuracy of the result simulated based on the MCM is very high. To investigate the effect of the randomness inherent to MCM, the time-resolved transient hemispherical reflectance was simulated for 15 times. The largest standard deviation obtained was less than 5.422×10^{-7}. Thus, the result simulated based on the MCM can be used as the measured value in the inverse analysis.

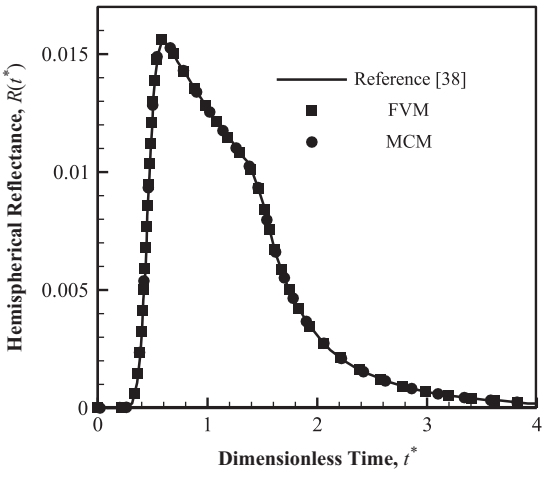

Fig. 5. Time-resolved hemispherical reflectance $R(t^*)$ versus the dimensionless time t^* comparing with Ref. [38].

Considering the fact that the direct problem model is needed to be solved for a large number of times during the inverse process, and unfortunately, the efficiency of the MCM is low, thus, it is unsuitable to be used as the solving model for the direct problem. On the contrast, the efficiency of FVM approximation is much higher than that of the MCM, so the FVM approximation is adopted as the solving model of the direct problem.

In FVM approximation, too many grids will occupy too much computation time. In order to improve the computation efficiency, the grid independence of the results was discussed under certain accuracy. Take the result simulated by FVM with $N_x=5000$, $N_\theta=100$ and $\Delta t_{fvm}^*=0.0001$ as a reference. Fig. 6(a) shows the effect of the number of grids, which increased from 5 to 3000 under the condition with the dimensionless time step $\Delta t_{fvm}^*=0.04$ and the number of the polar angle $N_\theta=10$. It can be seen from the figure that when the number is higher than 300, the declines of the maximum relative error and absolute error

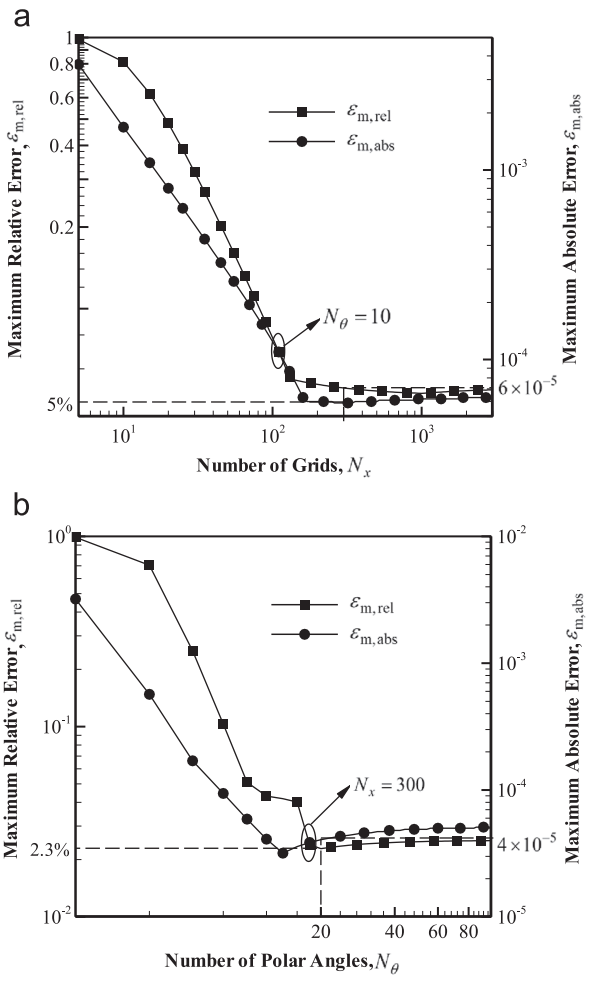

Fig. 6. The maximum relative error and absolute error for (a) different number of grids N_x and (b) different number of polar angles N_θ with $\Delta t_{fvm}^*=0.04$, $t_p^*=0.15$.

are slow. If we keep the dimensionless time step as $\Delta t^*_{fvm}=0.04$ and the number of grids as $N_x=300$, the number of the polar angle increases from 2 to 100, the result is shown in Fig. 6(b). When the number of the polar angle is larger than 20, the declines of the maximum relative error and absolute error are not obvious. The absolute error is less than 4×10^{-5}, and the relative error is less than 2.3%, which satisfied the requirement of the accuracy. Thus we used the FVM approximation as the solving model of the direct problem with $N_x=300$, $N_\theta=20$ and $\Delta t^*_{fvm}=0.04$.

The maximum relative error and the maximum absolute error are defined as follows:

$$\varepsilon_{m,\,abs}=\max\{|z_l-z_l^*|\times100\}\quad l=1,\,2,\ldots,\,N_l \tag{20}$$

$$\varepsilon_{m,\,rel}=\max\left\{\frac{|z_l-z_l^*|}{z_l^*}\times100\right\}\quad l=1,\,2,\ldots,\,N_l \tag{21}$$

In the model depicted in Section 4.1, four characteristic combinations of optical thickness and scattering albedo were investigated: (1) $\tau_L^*=0.3$, $\omega^*=0.5$; (2) $\tau_L^*=0.456$, $\omega^*=0.789$; (3) $\tau_L^*=0.8$, $\omega^*=0.998$; (4) $\tau_L^*=0.9$, $\omega^*=0.3$. The optical thickness and scattering albedo were retrieved simultaneously by measuring the time-resolved hemispherical reflectance. The MCM was used to solve the time-resolved hemispherical reflectance in $t^*<10$, the results are shown in Fig. 7. As shown in Fig. 7, the reflectance is too small when the dimensionless time $t^*>4$, thus the uniformly spaced 100 points within $t^*<4$ are chosen as the measurement positions.

After determining the measurement positions, the measured and estimated values can be calculated by MCM and FVM. Then we can apply the ACO-based algorithms to the transient radiative transfer problem by using Eq. (8). The objective function in Eq. (8) is defined as

$$O^k(t)=\frac{1}{100}\sum_{l=1}^{100}(z_l^k(t)-z_l^*)^2 \tag{22}$$

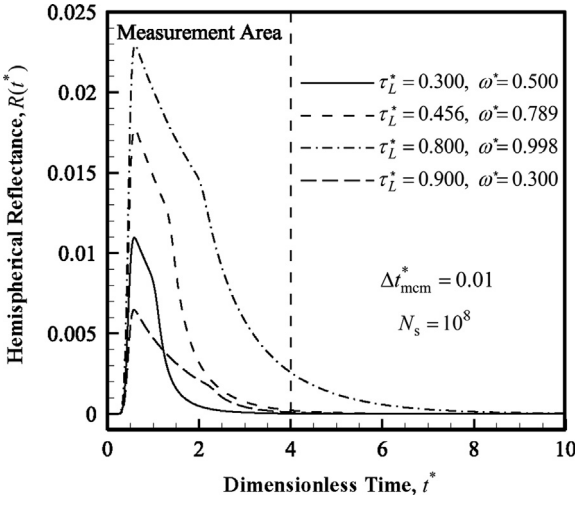

Fig. 7. Time-resolved hemispherical reflectance $R(t^*)$ versus the dimensionless time t^* with $t_p^*=0.15$ by MCM.

Table 1
The recommended system control parameters of ACO algorithms.

Control parameters	Nm	Nn	α	β	ρ	ζ	Q
Recommended value	30	8	1	2	0.7	0.3	10

where $z_l^k(t)$ and z_l^* means the measured value and estimated value at the lth measurement position, respectively.

4.3. Inverse problem

The system control parameters of the ACO algorithms have a great influence on the accuracy, efficiency and convergence. There are complex coupling relationships between these parameters. Furthermore, the parameters of ACO are more or less related to the direct problem. It is difficult to give the best values exactly. Of course, there are certain relations between these control parameters and the influence. Many scholars have studied these relationships and found some regulations. In this study, these parameters were obtained through a great deal of computation based on references [37,39,40]. For the inverse transient radiation problems in this paper, the system control parameters of the ACO algorithms were set as shown in Table 1.

By considering the fact that the ant colony algorithm is a stochastic search optimization method, and every optimization has certain randomness, each of these four ACO algorithms mentioned above are repeated 100 times for the model depicted in Section 4.1 with the four combinations of inversed parameters. The calculation results are shown in Table 2 in which the setting accuracy of the objective function was set as $\varepsilon=10^{-10}$, the size limit of the subinterval of the hunting zone was set as $\xi=10^{-5}$, the user-defined iteration limit was set as $N_c=1000$, the initial search space of τ_L and ω were set as [0, 1] and [0, 1]. The estimated value was simulated by FVM, and the measured value was simulated by MCM.

It can be seen from Table 2 that the accuracies of retrieved parameter and the efficiencies of the computation using the three improved ACO algorithms are much higher than that using the BACO algorithm. Due to modifying the reducing rule of hunting zone in the RACO algorithm, the probability of true value jumping out of the hunting zone is reduced. For the SACO algorithm, the probability of finding the true value has been further improved by adding a few stochastic ants. Furthermore, by adding homogenous factor, the HACO algorithm effectively inhibits the local convergence in earlier stage, and the accuracy of the inversed parameter is improved obviously.

It can also be seen from Table 2, the retrieved parameters of combination No. 4 ($\tau_L^*=0.9$, $\omega^*=0.3$) are less accurate than combination No. 1 ($\tau_L^*=0.3$, $\omega^*=0.5$), No. 2 ($\tau_L^*=0.456$, $\omega^*=0.789$) and No. 3 ($\tau_L^*=0.8$, $\omega^*=0.998$). In order to explain the retrieval characteristics of the four combinations clearly, the distributions of the objective function value with different ω and τ_L are shown in Fig. 8. As can be seen from Fig. 8, the region with minimum value of objective function is too big in combination No. 4,

Table 2
The expectation and standard deviation of the results using the ACO algorithms.

		BACO	RACO	SACO	HACO
1	$\tau_L^*=0.300$	$0.302\pm5.23\times10^{-3}$	$0.300\pm4.18\times10^{-4}$	$0.300\pm8.07\times10^{-5}$	$0.300\pm6.32\times10^{-5}$
	$\omega^*=0.500$	$0.499\pm5.28\times10^{-3}$	$0.500\pm5.05\times10^{-4}$	$0.500\pm7.72\times10^{-5}$	$0.500\pm7.01\times10^{-5}$
	Time/s	100.0 ± 31.5	71.3 ± 30.0	67.7 ± 22.3	68.8 ± 21.9
2	$\tau_L^*=0.456$	$0.461\pm1.36\times10^{-2}$	$0.456\pm2.42\times10^{-4}$	$0.456\pm2.29\times10^{-4}$	$0.456\pm1.03\times10^{-4}$
	$\omega^*=0.789$	$0.783\pm2.11\times10^{-2}$	$0.789\pm3.08\times10^{-4}$	$0.789\pm2.91\times10^{-4}$	$0.789\pm9.90\times10^{-5}$
	Time/s	76.4 ± 31.9	68.9 ± 21.1	74.7 ± 26.7	75.1 ± 19.6
3	$\tau_L^*=0.800$	$0.816\pm4.50\times10^{-2}$	$0.806\pm1.01\times10^{-2}$	$0.805\pm6.06\times10^{-3}$	$0.801\pm2.74\times10^{-3}$
	$\omega^*=0.998$	$0.986\pm2.11\times10^{-2}$	$0.996\pm2.64\times10^{-3}$	$0.997\pm1.95\times10^{-3}$	$0.998\pm7.90\times10^{-4}$
	Time/s	99.5 ± 31.5	96.6 ± 32.8	94.0 ± 32.3	84.5 ± 34.9
4	$\tau_L^*=0.900$	$0.889\pm3.93\times10^{-2}$	$0.894\pm1.63\times10^{-2}$	$0.894\pm1.51\times10^{-2}$	$0.897\pm1.31\times10^{-2}$
	$\omega^*=0.300$	$0.300\pm3.74\times10^{-3}$	$0.300\pm4.03\times10^{-4}$	$0.300\pm4.61\times10^{-4}$	$0.300\pm3.53\times10^{-4}$
	Time/s	98.5 ± 25.3	92.2 ± 36.0	91.2 ± 34.3	76.9 ± 36.1

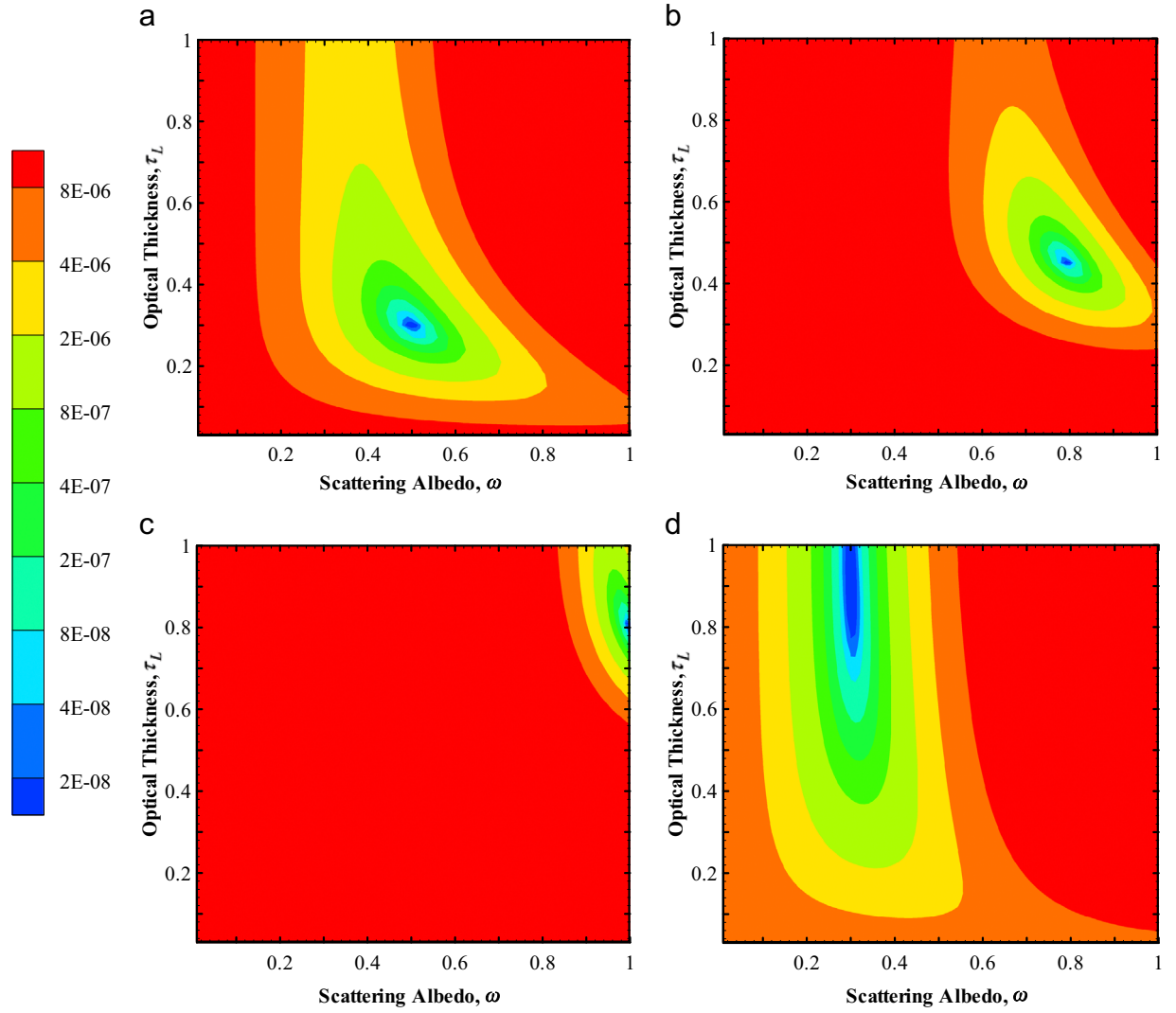

Fig. 8. The distribution of the objective function value with different inversed parameters when $0<\tau_L<1$, $0<\omega<1$. (a) with $\tau_L^*=0.300$, $\omega^*=0.500$, (b) with $\tau_L^*=0.456$, $\omega^*=0.789$, (c) with $\tau_L^*=0.800$, $\omega^*=0.998$ and (d) with $\tau_L^*=0.900$, $\omega^*=0.300$.

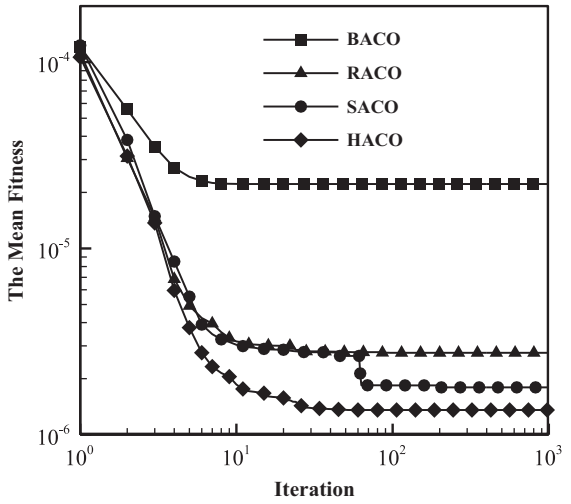

Fig. 9. The mean fitness versus iteration for 100 times computation with $\tau_L^* = 0.456$ and $\omega^* = 0.789$.

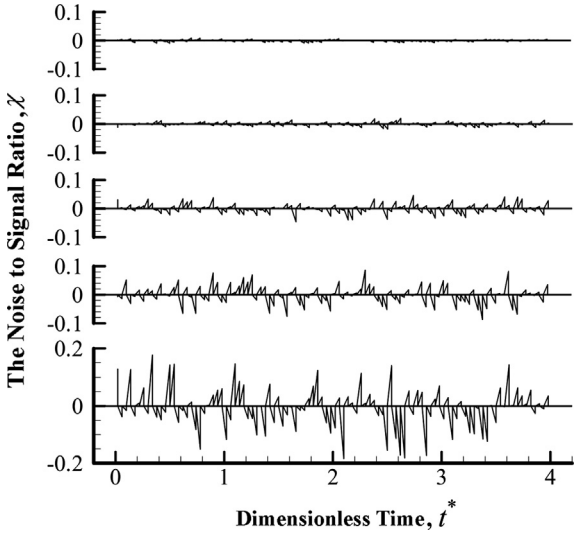

Fig. 10. The noise to signal ratio versus dimensionless time with the measured errors $\gamma = 1,\ 2,\ 5,\ 10,\ 20$.

which means that there exist a multi-value zone during the procedure of searching the true values, *i.e.*, there may be many couples of ω and τ_L values corresponding to the same measured time-resolved reflectance.

In order to investigate the convergence rule of the ACO algorithms, each algorithm is iterated for 1000 times. Taking the combination No. 2 as an example, the optical thickness and scattering albedo are set as $\tau_L^* = 0.456$ and $\omega^* = 0.789$, respectively. Each algorithm is implemented for 100 times to reduce the random error. The mean value of the minimum of the objective function, which is also called fitness, versus the iteration is shown in Fig. 9. It can be seen from Fig. 9 that the proposed approach HACO is more efficient and accurate than BACO, RACO and SACO algorithms.

To demonstrate the effects of measured errors on the predicted terms, random errors are considered. Measured time-resolved reflectance with random errors is obtained by adding normal distribution errors to the exact reflectance, as shown below:

$$z_l^* = z_{l,exa}^* + rand_n \sigma_l, \quad (l = 1,\ 2,\ \ldots,\ N_l) \tag{23}$$

where z_l^* is the noise-corrupted measured value in the lth position, $z_{l,exa}^*$ is the exact value of the measured value in the lth position, $rand_n$ is a normal distributed random variable with zero mean and unit standard deviation. The standard deviation of measured value σ_l, for a measured error of $\gamma\%$ at 99% confidence, is determined as

$$\sigma_l = \frac{z_{l,exa}^* \gamma\%}{2.576} \tag{24}$$

where 2.576 arises from the fact that 99% of a normally distributed population is contained within ± 2.576 standard deviation of the mean. The noise to signal ratio can be defined as

$$\chi_l = \frac{z_l^* - z_{l,exa}^*}{z_{l,exa}^*} \tag{25}$$

To further illustrate the performance of the HACO algorithm, measured value with $\gamma\%$ noise are used to estimate optical thickness and scattering albedo, where the measured error $\gamma\%$ are set as 1%, 2%, 5%, 10% and 20%, respectively, and the distributions of the noise to signal ratio are shown in Fig. 10. To reduce the effect of the random error inherent to the HACO algorithm, it was simulated for 100 times. The results were shown in Table 3, where the relative error was defined as

$$\varepsilon_{rel} = 100 \times \frac{\overline{Y} - Y_{exa}}{Y_{exa}} \tag{26}$$

where $\overline{Y}$ denotes the mean value of the retrieved variable, and Y_{exa} denotes the true value of the inversed parameter.

As can be seen from Table 3, the relative error of the inversed parameters increases with the increase of the measured error. The retrieved parameters are very close to the true value using HACO, even with a measured error of 20%. The maximum relative error of the inversed parameters is less than 2%, which proves that the HACO algorithm has a strong robustness.

5. Conclusions

The ACO algorithm was applied to the inverse transient radiation problem in this paper. It was adopted to optimize the parameters by minimizing an objective function, which is the sum of the square errors between the estimated and measured reflectance. By modifying the reducing rule of the hunting zone, adding some stochastic ants and the homogeneous factor, three improved ACO algorithms were developed based on the BACO algorithm. The inverse transient radiation analyses were carried out for retrieving the optical thickness and scattering albedo in a homogeneous absorbing and isotropic scattering but non-emitting plane-parallel slab. The improved ACO algorithms were demonstrated to be superior to the BACO algorithm in both accuracy and efficiency. Meanwhile, the

Table 3
The influence of measured errors on the retrieval results of the HACO algorithm.

Retrieved parameter	Y_{exa}	$\gamma=0$		$\gamma=1$		$\gamma=2$		$\gamma=5$		$\gamma=10$		$\gamma=20$	
		Y	εrel	Y	εrel	Y	εrel	Y	εrel	Y	εrel	Y	εrel
τL	0.300	0.300	0.00	0.300	0.00	0.300	0.00	0.299	−0.33	0.298	−0.67	0.299	−0.33
ω	0.500	0.500	0.00	0.500	0.00	0.502	0.40	0.501	0.20	0.504	0.80	0.504	0.80
τL	0.456	0.456	0.00	0.456	0.00	0.456	0.00	0.455	−0.22	0.463	1.54	0.464	1.75
ω	0.789	0.789	0.00	0.788	−0.13	0.790	0.13	0.788	−0.13	0.779	−1.27	0.794	0.63
τL	0.800	0.801	0.13	0.803	−0.38	0.804	0.50	0.806	0.75	0.812	1.50	0.814	1.75
ω	0.998	0.996	−0.20	0.997	−0.10	0.997	−0.10	0.997	−0.10	0.997	−0.10	0.995	−0.30
τL	0.900	0.897	−0.33	0.895	−0.56	0.891	−1.00	0.887	−1.44	0.884	−1.78	0.882	−2.00
ω	0.300	0.300	0.00	0.300	0.00	0.300	0.00	0.301	0.33	0.299	−0.33	0.302	0.67

inversed parameters can be estimated accurately even with noisy data by using the HACO algorithm. In conclusion, the improved HACO algorithms are demonstrated to be fast and robust, which have the potential to be implemented to solve various inverse radiation problems. Further study will focus on improving the performance of the ACO-based methodology and applying it to other multi-dimensional radiative inverse analysis in participating media.

Acknowledgments

The support of this work by the Foundation for Innovative Research Groups of the National Natural Science Foundation of China (No. 51121004), National Nature Science Foundation of China (No. 51076037), and the Specialized Research Fund for the Doctoral Program of Higher Education (No. 20122302110046) are gratefully acknowledged.

References

[1] Qi H, Ruan LM, Zhang HC, Wang YM, Tan HP. Inverse radiation analysis of a one-dimensional participating slab by stochastic particle swarm optimizer algorithm. Int J Therm Sci 2007;46(7):649–61.
[2] Qi H, Ruan LM, Wang SG, Shi M, Zhao H. Application of multi-phase particle swarm optimization technique to retrieve the particle size distribution. Chin Opt Lett 2008;6(5):346–9.
[3] Qi H, Ruan LM, Shi M, An W, Tan HP. Application of multi-phase particle swarm optimization technique to inverse radiation problem. J Quant Spectrosc Radiat Transfer 2008;109(3):476–93.
[4] Wang F, Liu D, Cen KF, Yan JH, Huang QX, Chi Y. Efficient inverse radiation analysis of temperature distribution in participating medium based on backward Monte Carlo method. J Quant Spectrosc Radiat Transfer 2008;109(12):2171–81.
[5] Liu D, Yan JH, Wang F, Huang QX, Chi Y, Cen KF. Inverse radiation analysis of simultaneous estimation of temperature field and radiative properties in a two-dimensional participating medium. Int J Heat Mass Transfer 2010;53(21):4474–81.
[6] Rukolaine SA. The shape gradient of the least-squares objective functional in optimal shape design problems of radiative heat transfer. J Quant Spectrosc Radiat Transfer 2010;111(16):2390–404.
[7] Qi H, Wang DL, Wang SG, Ruan LM. Inverse transient radiation analysis in one-dimensional non-homogeneous participating slabs using particle swarm optimization algorithms. J Quant Spectrosc Radiat Transfer 2011;112(15):2507–19.
[8] Liu D, Yan JH, Wang F, Huang QX, Chi Y, Cen KF. Experimental reconstructions of flame temperature distributions in laboratory-scale and large-scale pulverized-coal fired furnaces by inverse radiation analysis. Fuel 2012;93(1):397–403.
[9] Cui M, Gao XW, Chen HG. A new inverse approach for the equivalent gray radiative property of a non-gray medium using a modified zonal method and the complex-variable-differentiation method. J Quant Spectrosc Radiat Transfer 2011;112(8):1336–42.
[10] Zhao SY, Zhang BM, Du SY. An inverse analysis to determine conductive and radiative properties of a fibrous medium. J Quant Spectrosc Radiat Transfer 2009;110(13):1111–23.
[11] An W, Ruan LM, Qi H. Inverse radiation problem in one-dimensional slab by time-resolved reflected and transmitted signals. J Quant Spectrosc Radiat Transfer 2007;107(1):47–60.
[12] Salinas CT. Inverse radiation analysis in two-dimensional gray media using the discrete ordinates method with a multidimensional scheme. Int J Therm Sci 2010;49(2):302–10.
[13] Mattingly J, Mitchell DJ. A framework for the solution of inverse radiation transport problems. IEEE Trans Nucl Sci 2010;57(6):3734–43.
[14] Grissa H, Askri F, Ben SM, Ben NS. Efficient inverse radiation analysis in a participating cylindrical medium. High Temp–High Pressures 2012;41(1):23–37.
[15] Goldberg DE, Holland JH. Genetic algorithms and machine learning. Mach Learn 1988;3(2):95–9.
[16] Das R, Mishra SC, Ajith M, Uppaluri R. An inverse analysis of a transient 2-D conduction-radiation problem using the lattice Boltzmann method and the finite volume method coupled with the genetic algorithm. J Quant Spectrosc Radiat Transfer 2008;109(11):2060–77.
[17] Lee KH, Baek SW, Kim KW. Inverse radiation analysis using repulsive particle swarm optimization algorithm. Int J Heat Mass Transfer 2008;51(11–12):2772–83.
[18] Farahmand A, Payan S, Sarvari SMH. Geometric optimization of radiative enclosures using PSO algorithm. Int J Therm Sci 2012;60:61–9.
[19] Poli R, Kennedy J, Blackwell T. Particle swarm optimization. Swarm Intell 2007;1(1):33–57.
[20] Colorni A, Dorigo M, Maniezzo V. Distributed optimization by ant colonies. In: Proceedings of the first European conference on artificial life. Paris, France; 1991. p. 134–42.
[21] Gutjahr WJ. A graph-based ant system and its convergence. Future Gener Comput Syst 2000;16(8):873–88.
[22] Bonabeau E, Dorigo M, Theraulaz G. Inspiration for optimization from social insect behaviour. Nature 2000;406(6791):39–42.
[23] Dorigo M, Stützle T. Ant colony optimization. Cambridge: Massachusetts Institute of Technology Press; 2004.
[24] Bai J, Yang GK, Chen YW, Hu LS, Pan CC. A model induced max–min ant colony optimization for asymmetric traveling salesman problem. Appl Soft Comput 2013;13(3):1365–75.
[25] Zhou XF, Wang RL. Self-evolving ant colony optimization and its application to traveling salesman problem. Int J Innovative Comput Inf Control 2012;8(12):8311–21.
[26] Kokilavani T, Amalarethinam DIG. An ant colony optimization based load sharing technique for meta task scheduling in grid computing. Adv Comput Inf Technol 2013;177(2):395–404.
[27] Li DW, Zhang RR, Wang L. On the batch scheduling problem in steel plants based on ant colony algorithm. In: Proceedings of the 2012 international conference of modern computer science and applications, Berlin, 2013. Berlin: Springer-Verlag; 2013. p. 645–50.
[28] Lu CF, Hsu CH, Juang CF. Coordinated control of flexible ac transmission system devices using an evolutionary fuzzy lead-lag controller with advanced continuous ant colony optimization. IEEE Trans Power Syst 2013;28(1):385–92.

[29] Ataie AB, Ketabchi H. Elitist continuous ant colony optimization algorithm for optimal management of coastal aquifers. Water Resour Manage 2011;25(1):165–90.
[30] Otero FEB, Freitas AA, Johnson CG. Inducing decision trees with an ant colony optimization algorithm. Appl Soft Comput 2012;12(11):3615–26.
[31] Wu MT, Hong TP, Lee CN. A continuous ant colony system framework for fuzzy data mining. Appl Soft Comput 2012;16(12):2071–82.
[32] Bozdogan AO, Efe M. Improved assignment with ant colony optimization for multi-target tracking. Expert Syst Appl 2011;38(8):9172–8.
[33] D'Acierno L, Gallo M, Montella B. An ant colony optimization algorithm for solving the asymmetric traffic assignment problem. Eur J Oper Res 2012;217(2):459–69.
[34] Rizk C, Arnaout JP. ACO for the surgical cases assignment problem. J Med Syst 2012;36(3):1891–9.
[35] Blum C. Ant colony optimization: introduction and recent trends. Phys Life Rev 2005;2(4):353–73.
[36] Dorigo M, Caro GD, Gambardella LM. Ant algorithms for discrete optimization. Artif Life 1999;5(2):137–72.
[37] Duan HB, Wang DB, Zhu JQ. Novel method based on ant colony optimization for solving ill-conditioned linear systems of equations. J Syst Eng Electron 2005;16(3):606–10.
[38] Smith KD, Katika KM, Pilon L. Maximum time-resolved hemispherical reflectance of absorbing and isotropic scattering media. J Quant Spectrosc Radiat Transfer 2007;104(3):384–99.
[39] Chen Y, Feng J, Wu YF. Prestress stability of pin-jointed assemblies using ant colony systems. Mech Res Commun 2012;41:30–6.
[40] Hu XM, Zhang J, Chung SH, Li Y, Liu O. SamACO: variable sampling ant colony optimization algorithm for continuous optimization. IEEE Trans Syst Man Cybern—Part B: Cybern 2010;40(6):1555–66.